Finite-temperature analysis of a quasi-two-dimensional dipolar gas

Christopher Ticknor
Theoretical Division, Los Alamos National Laboratory, Los Alamos, New Mexico 87545, USA
(Received 13 February 2012; published 22 March 2012)

We present a finite-temperature analysis of a quasi-two-dimensional (Q2D) dipolar gas. To do this, we use the Hartree-Fock-Bogoliubov method within the Popov approximation. This formalism is a set of nonlocal equations containing the dipole-dipole interaction and the condensate and thermal correlation functions, which are solved self-consistently. We detail the numerical method used to implement the scheme. We present density profiles for a finite-temperature dipolar gas in Q2D and compare these results to those for a gas with zero-range interactions. Additionally, we analyze the excitation spectrum and study the impact of the thermal exchange.

DOI: 10.1103/PhysRevA.85.033629 PACS number(s): 03.75.Hh, 67.85.−d

I. INTRODUCTION

Two popular topics in ultracold physics are two-dimensional (2D) gases and dipolar gases. Reduced dimensionality enhances the quantum-mechanical character of the system. In a homogeneous 2D system, quantum phase fluctuations are so strong that at finite temperature phase coherence cannot be established and condensation does not occur. There is, however, an intriguing phase transition called the Berezinskii-Kosterlitz-Thouless (BKT) transition [1] which occurs when the temperature is lowered and there is no longer enough thermal energy to unbind vortex and antivortex pairs. This binding of vortices reduces phase fluctuations so that quasi-long-range order can form [2]. Interestingly, a trapped 2D gas can form a Bose-Einstein condensate (BEC) at finite temperature [2,3]. The BKT and BEC transitions have been studied in trapped ultracold gases, first by observations of phase defects [4] and direct observation of vortices [5], and then by changes in the density profile due to the onset of superfluidity [6]. Additionally, universality has been observed near the BKT transition [7]. Successful methods used to study such systems are Monte Carlo simulation [8,9] and mean-field [10–12] and classical-field [13–15] methods.

In dipolar systems the interactions are nonlocal and the possibility of creating strongly correlated gases is tantalizing, especially in quasi-2D (Q2D) where zero-point motion in the axial direction is included. For example, some studies have used Monte Carlo methods to study phase transitions such as crystallization [16]. This study included temperature as a variable and observed melting of the dipolar crystal. The BKT transition of a homogeneous dipolar gas has been studied with Monte Carlo methods to examine the superfluid fraction and excitation spectra [17]. Other studies have looked at the structure of the dipolar gas and the impact of temperature on the phase of the gas [18,19]. Such studies have focused on strongly interacting dipolar systems. However, the bulk of the work on Q2D gases has been at zero temperature. For example, phonon instability [20] and anisotropic superfluidity [21] have been predicted.

Recently, chromium (Cr) and dysprosium (Dy) have been Bose-Einstein condensed and exhibited strong dipolar effects [22,23]. Additionally, progress toward a Q2D dipolar gas has been made with a layered dipolar system for Cr atoms in a one-dimensional optical lattice [24]. With such progress on dipolar gases, direct study of Q2D dipolar systems has begun. An important question is how dipolar interactions impact the quantum behavior of a Q2D gas. The long-range nature of the dipolar interaction may lead to interesting physics for the thermal system, especially relating the BKT transition and phase coherence. Additionally, little work studying the impact of temperature on Q2D dipolar gases has been conducted for reasonable experimental parameters.

With an eye toward this unexplored physics and aiding experiments, we study the finite-temperature physics of Q2D trapped dipolar gases. We use the standard beyond-mean-field method: the Hartree-Fock-Bogoliubov method within the Popov (HFBP) approximation [25]. The HFBP approximation has been successful in studying ultracold atoms; for example, it has been used to explain the temperature dependence of collective excitations in a 3D BEC [26]. In the case of 3D dipolar gases, the authors of Refs. [27] used the HFBP method to study temperature effects on the biconcave structure dipolar gases can have [28]. This study neglected the thermal exchange. Other recent work used mean-field methods to study the stability of finite-temperature dipolar gases [29].

The aim of this paper is twofold. First, we develop a numerical method to solve the nonlocal HFBP problem. This method includes the nonlocal interaction and exchange effects. We show in detail how the interaction and thermal exchange effects are included; this relies on a parallel implementation of the method. The method can also be applied to dipolar fermions. Second, we compare the contact gas and the dipolar gas with the HFBP method. In the comparison of the two gases, we look at the condensate number as a function of temperature. We also articulate the role of thermal exchange in the gas by solving the system with and without thermal exchange. We compare the density profiles of the gas at various temperatures. We look at the excitation spectrum as a function of both temperature and total particle number. We also classify the lowest excitation modes. We present results for a Q2D trapped finite-temperature dipolar gas with thermal exchange effects.

II. EQUATIONS OF MOTION

We study a quasi-2D dipolar system at finite temperature. To do this, we will employ the Hartree-Fock-Bogoliubov method within the Popov approximation with nonlocal interactions [25,30]. The HFB method breaks the second-quantized bosonic field operator into condensate and noncondensate

(thermal) components: $\hat{\Psi} = [\sqrt{N_0}\phi_0(x) + \hat{\theta}(x)]$ where we have replaced $\hat{a}_0 \to \sqrt{N_0}$. Here x represents all required coordinates; for the 2D case it will be $\vec{\rho}$. We will use the Bogoliubov transformation for the thermal part: $\hat{\theta}(x) = \sum_\alpha [u_\alpha(x)\hat{a}_\alpha e^{-i\omega_\alpha t} - v^*_\alpha(x)\hat{a}^*_\alpha e^{i\omega_\alpha t}]$ where $\hat{a}$ ($\hat{a}^*$) is the bosonic annihilation (creation) operator for a quasiparticle (quasihole). They obey the bosonic commutation relations: $[\hat{a}_\alpha,\hat{a}^*_\beta] = \delta_{\alpha\beta}$ and $[\hat{a}_\alpha,\hat{a}_\beta] = [\hat{a}^*_\alpha,\hat{a}^*_\beta] = 0$. To derive the equations of motion we start with the Heisenberg equation of motion with a nonlocal interaction [30]. We find for our system that the modified non-local Gross-Pitaevskii equation (GPE) is

$$\mu\phi_0(x) = \left(H_0 + \int dx' n(x')V\right)\phi_0(x) + \int dx'[\tilde{n}(x,x') - \tilde{m}(x,x')]V\phi_0(x'), \quad (1)$$

where H_0 is the kinetic energy and trapping potential. The interaction potential $V(x-x')$ has been written as V for simplicity. The total density $n(x) = n_0(x) + \tilde{n}(x)$ is made up of the condensate density and thermal density. The nonlocal correlation functions are $n_0(x,x') = N_0\phi^*_0(x)\phi_0(x')$ and $n_0(x) = n_0(x,x)$; $\tilde{n}(x,x') = \langle\hat{\theta}^*(x)\theta(x')\rangle$ is the thermal correlation function and the local thermal density is $\tilde{n}(x) = \tilde{n}(x,x)$. $\tilde{m}(x,x') = \langle\hat{\theta}(x)\hat{\theta}(x')\rangle$ is the anomalous thermal correlation function, and in the Popov approximation it is neglected. The quasiparticle wave functions are required to construct the thermal and anomalous correlation functions. At equilibrium, these wave functions can be found from a nonlocal Bogoliubov–de Gennes equation:

$$\begin{aligned}
\omega_\alpha u_\alpha(x) &= \left(H_0 - \mu + \int dx' n(x')V\right)u_\alpha(x) \\
&\quad + \int dx'[n_0(x,x') + \tilde{n}(x,x')]Vu_\alpha(x') \\
&\quad + \int dx'\tilde{m}(x,x')Vv_\alpha(x') - \int dx' m_0(x,x')Vv_\alpha(x'), \\
-\omega_\alpha v_\alpha &= \left(H_0 - \mu + \int dx' n(x')V\right)v_\alpha(x) \\
&\quad + \int dx'[n_0(x,x') + \tilde{n}(x,x')]Vv_\alpha(x') \\
&\quad + \int dx'\tilde{m}^*(x,x')Vu_\alpha(x') - \int dx' m^*_0(x,x')Vu_\alpha(x').
\end{aligned} \quad (2)$$

The total number of atoms is $N = N_0 + \tilde{N}$ and $\tilde{N} = \int dx\tilde{n}(x)$. The normalization of the quasiparticle wave function is $1 = \int dx(|u_\alpha|^2 - |v_\alpha|^2)$. The anomalous condensate correlation function is $m_0(x,x') = N_0\phi(x)\phi(x')$. The thermal correlation functions are defined in terms of the quasiparticles:

$$\tilde{n}(x,x') = \sum_\alpha [u^*_\alpha(x')u_\alpha(x) + v_\alpha(x')v^*_\alpha(x)]N^\alpha_{\rm BE} + v_\alpha(x')v^*_\alpha(x), \quad (3)$$

$$\tilde{m}(x,x') = \sum_\alpha [u_\alpha(x')v^*_\alpha(x) + v^*_\alpha(x')u_\alpha(x)]N^\alpha_{\rm BE} + u_\alpha(x')v^*_\alpha(x). \quad (4)$$

Here $N^\alpha_{\rm BE} = (Ze^{\hbar\omega_\alpha/kT} - 1)^{-1} = \langle\hat{a}^*_\alpha\hat{a}_\alpha\rangle$, where k is Boltzmann's constant, T is the temperature, and $Z = 1 + 1/N_0$. This relation is simply the bosonic occupation of thermal modes. These equations are consistent with Refs. [27,30,31] when the appropriate simplification is made.

To make the discussion of Eqs. (1) and (2) simpler, we introduce a compact notation:

$$(H_0 + D + \tilde{X} + \tilde{M})\phi_0 = \mu\phi_0, \quad (5)$$

$$\begin{aligned}
(H_0 - \mu + D + X)u_\alpha + Mv_\alpha &= \omega_\alpha u_\alpha, \\
(H_0 - \mu + D + X)v_\alpha + Mu_\alpha &= -\omega_\alpha v_\alpha.
\end{aligned} \quad (6)$$

The first term is the standard kinetic and potential energy, H_0. For the remaining interaction terms, we use the capital letters to indicate the inclusion of the x' integral, so the direct interaction is $D = D_0 + \tilde{D}$ (condensate and thermal), and for example $D_0(x) = \int dx'[n_0(x')]V(x-x')$. The exchange interaction is $X = X_0 + \tilde{X}$ (condensate and thermal), and for example $\tilde{X}(x,x') = \int dx'[\tilde{n}(x,x')]V(x-x')$. Finally, the anomalous correlation function is $M = \tilde{M} - M_0$, and for example $M(x,x') = \int dx'[\tilde{m}(x,x') - m_0(x,x')]V(x-x')$. We will use the Popov approximation, which assumes $\tilde{M} = 0$, leading to $M = -X_0$ if ϕ_0 is real. This approximation keeps the spectrum gapless.

We project out the condensate mode from the quasiparticles, as was done in Refs. [32,33], which use $Q = 1 - |0\rangle\langle 0|$ and $\langle x|0\rangle = \phi_0(x)$. The projection operator is applied to all operators that are not in $H_{\rm GP} = H_0 - \mu + D + \tilde{X}$, such as M_0 and X_0, and for example, $M_0 \to QM_0Q$. This projection method keeps the spectrum gapless.

III. THE INTERACTION

We are interested in the Q2D dipolar system assuming no axis of symmetry, so we take the dipole moment to be $\vec{d} = d[\hat{z}\cos(\alpha) + \hat{x}\sin(\alpha)]$, and we assume harmonic confinement and that $\omega_z \gg \omega_\rho$ where the ω_i are the trapping frequencies ($\omega_x = \omega_y = \omega_\rho$). This allows us to assume that only one transverse mode is occupied in the z direction. We can then evaluate the interaction by factoring the wave function as $\psi(\vec{r}) = \chi_0(z)\psi(\vec{\rho})$, where ψ is either ϕ_0, u_α, or u_α and χ_0 is an eigenstate of H_0 in the z direction. We are then able to integrate out z and obtain an effective interaction. We will also consider a contact interaction. The interaction we use is

$$V(\vec{\rho}) = g\delta(\vec{\rho}) + g_d V_{dd}(\vec{\rho}), \quad (7)$$

where $g = \sqrt{8\pi}\hbar^2 a_s/ml_z$ is the strength of the contact interaction, a_s is the s-wave scattering length ($a_s \ll l_z$), $l_z = \sqrt{\hbar/m\omega_z}$ is the axial harmonic-oscillator length, $g_d = d^2/\sqrt{2\pi}l_z$, and d is the dipole moment of the particles. This interaction leads to the dipolar length scale: $l_d = md^2/\hbar^2$. In practice, we rescale the equations of motion into oscillator units, where the units of energy and length are $\hbar\omega_\rho$ and $l_\rho = \sqrt{\hbar/m\omega_\rho}$. After this rescaling, the dipolar interaction strength becomes $g_d = l_d/(l_z\sqrt{2\pi})$. Finally, the dipolar interaction

in Q2D is

$$V_{dd}(\vec{\rho}-\vec{\rho}') = \int dz \chi_0^2(z) \int dz' \chi_0^2(z') V_d^{3D}(\vec{r}-\vec{r}'),$$
$$V_{dd}^{3D}(\vec{r}) = d^2(1-3(\hat{d}\cdot\hat{r})^2)/r^3. \quad (8)$$

The interaction is evaluated in momentum space. As an example, the direct interaction is

$$D(\vec{\rho}) = \mathcal{F}^{-1}[n(\vec{k})\tilde{V}(\vec{k})],$$
$$\tilde{V}(\vec{k}) = g_d \frac{4\pi}{3} F\left(\frac{\vec{k}l_z}{\sqrt{2}}\right), \quad (9)$$

where $\mathcal{F}$ is the Fourier transform operator and $n(\vec{k}) = \mathcal{F}[n(\vec{\rho})]$. $\tilde{V}_k$ is the momentum representation of the interaction. The function $F(\vec{k})$ is the k-space dipolar interaction for the Q2D geometry. It has two contributions coming from polarization perpendicular to and in the direction of the dipole tilt, $F(\vec{k}) = \cos^2(\alpha)F_\perp(\vec{k}) + \sin^2(\alpha)F_\parallel(\vec{k})$ where α is the angle between $\hat{z}$ and the polarization vector $\hat{d}$. Its contributions are $F_\parallel(\vec{k}) = -1 + 3\sqrt{\pi}(k_d^2/k)e^{k^2}\mathrm{erfc}(k)$, where $\vec{k}_d$ is the wave vector along the polarization direction in the x-y plane, erfc is the complementary error function, and $F_\perp(\vec{k}) = 2 - 3\sqrt{\pi}ke^{k^2}\mathrm{erfc}(k)$ [20,21,34].

To evaluate the exchange interaction, we use a simple, yet memory-intensive, solution: we explicitly construct the interaction on the same space-space grid as the correlation functions. We put $n(\vec{\rho},\vec{\rho}')$ on a grid specified by the indices s and t, representing $\vec{\rho}$ and $\vec{\rho}'$. Each grid has n_s spatial points, and a correlation function has n_s^2 grid points.

To evaluate the interaction, we work in momentum space. The interaction on the space-space grid is

$$V_{st} = W_{sk}^T \tilde{V}_k W_{kt}, \quad (10)$$

where W_{ks} is the operator that transforms between the space (s) and k-space (k) representations via the spectral basis set [35]. The operator takes the place of the Fourier operator in our algorithm. An important aspect of the method is that it regularizes the interaction and avoids the logarithmic divergence as $\vec{\rho}\to\vec{\rho}'$ encountered by directly evaluating Eq. (8) because W_{kt} involves a projection onto the Gauss-Hermite basis set [35]. Construction of the interaction involves the most costly step, requiring n_s^3 operations per node. This is performed only once for a set of interaction parameters (l_z and α) and basis set size.

We have constructed a parallel implementation of the method. We distribute the s index ($\vec{\rho}$ grid) across the computing nodes (p); we will denote this distributed index as s_p. In this way, each core handles only a fraction of the correlation functions and interaction. In the future, we will construct the interaction in the partial wave expansion: $V(\vec{\rho}) = \sum_m V_m(\rho,\phi)$. This expansion will be necessary to handle an interaction which depends on quantum numbers such as n_z (confinement in z) or spin.

IV. NUMERICAL IMPLEMENTATION

We solve Eqs. (5) and (6) by expanding the wave functions on the basis that diagonalizes H_0. We will focus on the harmonically trapped case where $H_0\chi_\alpha = \epsilon_\alpha\chi_\alpha$, $\int d\vec{\rho}\chi_\alpha^*(\vec{\rho})\chi_\beta(\vec{\rho}) = \delta_{\alpha\beta}$, and $\epsilon_\alpha = \hbar\omega_\rho(m_x+m_y+1)$ where m_α is an integer. In a basis set, the evaluation of the direct interaction term $D_{\alpha\beta}$ is straightforward: $\int d\vec{\rho}\chi_\alpha(\vec{\rho})[\int dx' V(\vec{\rho}-\vec{\rho}')n(\vec{\rho}')]\chi_\beta(\vec{\rho})$, where the quantity in the square brackets is the effective potential from the interaction. The more complicated terms are the nonlocal exchange terms, such as the thermal exchange $\tilde{X}_{\alpha\beta}$, which is $\int d\vec{\rho}\chi_\alpha^*(\vec{\rho})\int d\vec{\rho}'\tilde{n}(\vec{\rho},\vec{\rho}')V(\vec{\rho}-\vec{\rho}')\chi_\beta(\vec{\rho}')$.

The nonlocal exchange term in the spectral basis is $X_{\alpha\sigma} = U_{\alpha s}^T V_{st} n_{st} U_{t\sigma}$, where $U_{s\sigma}$ is the transformation between the spectral basis (σ) and space basis (s). The numerical procedure to evaluate this on node p is as follows: (1) $Y_{s_pt} = V_{s_pt}n_{s_pt}$, multiply the interaction and correlation function; (2) $h_{s_p\sigma} = Y_{s_pt}U_{t\sigma}$, project the t spatial basis onto the σ spectral basis; (3) $X_{\alpha\sigma}^p = \sum_{s_p} U_{s_p\alpha}^T h_{s_p\sigma}$, project the s_p spatial basis onto the α spectral basis; and (4) $X_{\alpha\sigma} = \sum_p X_{\alpha\sigma}^p$, collect and sum. In comparison, the direct terms are straightforward and evaluated in momentum space at each step. $\Phi_s = W_{sk}\tilde{V}_k W_{kt} n_t$, where Φ_s is the effective potential. Then we must project onto the basis $D_{\alpha\sigma} = U_{\alpha s}^T \Phi_s U_{s\sigma}$, and this is done in parallel.

The procedure to find the full solution is as follows. Set the temperature T and N_0 and pick a targeted value for the total number of particles in the system N_{target}, and set $\tilde{n} = 0$ and $\tilde{m} = 0$:

(1) Solve Eq. (1) for ϕ_0 and μ (in the basis set).

(2) Construct the condensate exchange term X_0 with $n_0(\vec{\rho},\vec{\rho}')$ and put in the basis set.

(3) Solve Eq. (2) for u_α and v_α.

(4) Construct $\tilde{n}(\vec{\rho},\vec{\rho}')$ and $\tilde{m}(\vec{\rho},\vec{\rho}')$.

(5) Use the semiclassical local-density approximation (LDA) to supplement the thermal tail (see below), which gives $\tilde{N}$ and therefore $N = N_0 + \tilde{N}$.

(6) Construct thermal and anomalous exchange terms $\tilde{X}$ and $\tilde{M}$ (if not using the Popov approximation) and put them in the basis set representation.

(7) Adjust N_0 to get the desired N_{target} of atoms. We require N to be within 1% of N_{target}.

(8) Go back to step 1 until self-consistency is reached. We converge the number of thermal atoms, so that $|\tilde{n}_i - \tilde{n}_{i-1}| < 5\times10^{-5}$, when we are near enough N_{target}.

With the numerical method in hand, we are ready to proceed to the physical examples and the results.

The semiclassical LDA is very important for large-$\vec{\rho}$ and high-momentum states on the grid. At high temperature with a manageable grid size (much bigger than the condensate), we find that there can be an appreciable number of atoms outside the quadrature grid. For the large-$\vec{\rho}$ contributions, the density is low enough that the analytical, noninteracting solution can be used to account for these off-grid particles. We integrate the analytical solution over a large region outside the grid. We have tested that this does not impact the convergence of the end result. We include the impact of higher transverse modes in the same analytical manner on and off the grid. We also assume that these particles in the higher-z modes are noninteracting. This is reasonable, especially because symmetry prevents the first excited transverse mode from colliding with the condensate with $m = 0$ symmetry. Additionally, a noticeable number of thermal particles are in momentum states beyond the calculated quantum spectrum [36,37].

To include these thermal atoms we use the method from Ref. [27].

V. PHYSICAL EXAMPLES

We will study Cr and Dy atoms. These atoms have been Bose-Einstein condensed and shown to exhibit strong dipolar effects [22,23]. The first example we choose is 2×10^3 Cr atoms with $l_d = 45a_0$, where a_0 is the Bohr radius. This gives $g_d = 0.0028$ and $g = 0$ in trap units. Additionally, we pick $l_z/l_\rho = 0.1$; this is from using $(\omega_\rho,\omega_z) = 2\pi \times (16,1600)$ Hz. We have found that our numerical procedure converges using 465 basis states with an energy cut of $30\hbar\omega_\rho$. To compare this to a contact gas, we match the chemical potential at zero temperature by varying g. We will consider only $\alpha = 0$ here, that is, perpendicular polarization where the dipolar interaction is isotropic and repulsive. We also study Dy with a trapping potential of $(\omega_\rho,\omega_z) = 2\pi \times (10,1000)$ Hz. With $l_d = 400a_0$, this gives $g_d = 0.034$ in trap units. This is strongly interacting, and to maintain the Kohn mode (center-of-mass slosh mode), we have used a low atom number, and for our example we use 300 atoms [22]. It is important to note that the Cr example is very similar to recent experiments [24]. In that work, the authors were able to vary l_z/l_ρ between 0.1 and 0.17 and have up to 2000 atoms in a layer [24]. However, this is a layered system and interlayer dipolar interactions are important.

In contrast to a homogeneous system, a trapped ideal 2D gas can have Bose-Einstein condensation [3]. In this case, the critical temperature is at $T_{c0}/\hbar\omega = \sqrt{6N}/\pi \sim 0.78\sqrt{N}$. We will use this temperature to rescale our findings so that, to first order, we remove the number dependence of the results. This is important because, as we vary the temperature, we do not have exactly the same number of particles in every calculation. In the thermodynamic limit, the population of the condensate is $N_0/N = 1 - (T/T_{c0})^2$ [3].

For reference, we give several specific numerical examples in Table I. For two temperatures, we report μ, N_0/N, N, and the Kohn mode energy (which should be $1\hbar\omega_\rho$). For the Dy ($g_d = 0.034$) example, at $T/T_{c0} = 0.5$, the Kohn mode has noticably deviated from 1 by about 2.5%; this is about the worst the convergence of this mode gets as a function of temperature. For both dipolar examples, we show the results when thermal exchange is negelected ($\tilde{X} = 0$). The lower-temperature solutions are similar to the GPE solutions at $T = 0$.

TABLE I. Numerical examples of the HFBP for the Q2D dipolar gas and contact gas.

	T/T_{c0}	$\mu/\hbar\omega$	N_0/N	N	(Kohn-mode energy)/$\hbar\omega$
$g_d = 0.0028$	0.05	3.822	0.994	2004	0.9992
	0.5	3.457	0.658	1994	0.995
$g_d = 0.0028$	0.05	3.814	0.994	2004	0.9996
$\tilde{X} = 0$	0.5	3.341	0.660	1994	0.997
$g = 0.021$	0.05	3.829	0.993	2004	0.9991
	0.5	3.541	0.662	1993	0.9995
$g_d = 0.034$	0.05	5.124	0.983	300	0.991
	0.5	4.919	0.525	298	0.976
$g_d = 0.034$	0.05	5.094	0.983	300	0.996
$\tilde{X} = 0$	0.5	4.524	0.5500	303	0.987

VI. PROPERTIES OF A Q2D DIPOLAR GAS AT FINITE TEMPERATURE

In this section we study the properties of a Q2D dipolar gas at finite temperature, and compare it to a contact gas and a dipolar system without the thermal exchange. We look at several different aspects of these systems. First, we look at the condensate number as a function of temperature. Then we compare the interaction contributions to the total energy. Third, we compare the density profiles of the contact and dipolar gases, at various temperatures. Fourth, we look at the impact of including the thermal exchange on the density profile of the gas. Finally, we look at the excitation spectrum as a function of temperature and total particle number. We also classify the lowest excitation modes.

Figure 1 shows the condensate fraction for the Cr dipolar gas (black line with circles), the contact gas (green dash-dotted line), for 2000 ideal particles (solid black line), 300 Dy particles (dashed red line), and 300 ideal particles (red open squares). The condensate fractions for the dipolar gas and contact gas are shifted down from the ideal gas (black line), with the dipolar gas being slightly lower than the contact gas. For the Dy example, it is clear that the interaction strongly depletes the condensate mode.

In Fig. 2 we look at the chemical potential and its contributions from Eq. (1), as a function of temperature. The examples shown are dipolar (solid black), contact (dashed red), and dipolar without thermal exchange (dash-dotted blue). We show the direct condensate interaction ($\langle\phi_0|D_0|\phi_0\rangle/\mu$, triangles), the direct thermal interaction ($\langle\phi_0|\tilde{D}|\phi_0\rangle/\mu$, circles), and the thermal exchange interaction ($\langle\phi_0|\tilde{X}/|\phi_0\rangle/\mu$, squares). For the contact interaction, the thermal exchange is equal to thermal direct interaction, so we show only one. For each example, the remaining contribution to the chemical potential is from H_0 or the potential and kinetic energy contributions.

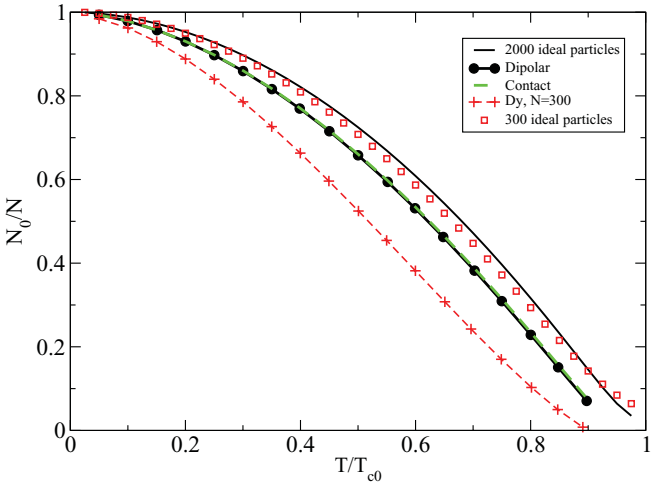

FIG. 1. (Color online) N_0/N as a function of temperature for the Cr dipolar gas (thick black line with circles), the contact gas (green dash-dotted line), and for 2000 ideal trapped particles (solid black line). Additionally, a gas of 300 Dy particles (dashed red with +) and one of 300 ideal particles (red open squares) are shown.

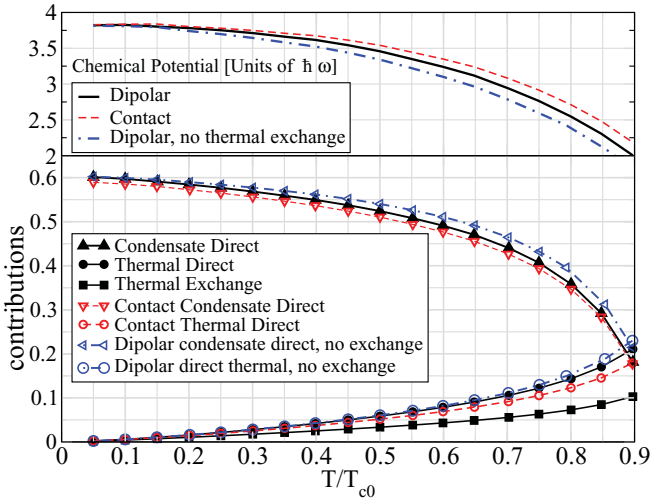

FIG. 2. (Color online) The chemical potential for three systems: dipolar (solid black), contact (dashed red), and dipolar without exchange (dash-dotted blue) and the interaction terms for each system in the Hamiltonian as a function of temperature. The contributing terms are the direct condensate ($\langle\phi_0|D_0|\phi_0\rangle/\mu$, triangles), the direct thermal ($\langle\phi_0|\tilde{D}|\phi_0\rangle/\mu$, circles), and the thermal exchange ($\langle\phi_0|\tilde{X}/|\phi_0\rangle/\mu$, squares) interactions.

For the dipolar gas, the thermal exchange term is about half as strong as the direct contribution. The importance of the interaction with the thermal particles is more important as the temperature is increased. Comparing the dipolar calculation with and without the thermal exchange, we see that the chemical potentials agree reasonably well; the full calculation has a larger μ at high temperature. Looking at the interaction contributions, we see that the direct condensate (black triangles) and thermal interaction (black circles) make up a smaller portion of the chemical potential for the full calculation than the one with $\tilde{X} = 0$ (blue triangles and open circles).

In Fig. 3 we show both the total and condensate density for (a) a Cr system of 2000 particles and (b) an analogous contact system (near equal chemical potentials). We then compare the total density profiles in Fig. 3(c). The total density is in blue (black) for the dipolar (contact) systems, and the condensate density is shown in red. The temperatures from top to bottom are $T/T_{c0} = 0.25$ (dashed), 0.55 (dotted), 0.75 (dash-dotted), and 0.90 (solid). For both the contact and dipolar gases at large ρ, the thermal density behaves as the analytical solution predicts.

An important point is that the dipolar gas has a higher density in the middle of the trap than the contact gas. It is hard to see in the figure, but the contact condensate atoms have been shifted to the shoulders of the condensate or near to the trap edge. This has implications for the temperature at which the superfluid phase transition will occur in a dipolar gas.

In Fig. 4 we compare both the total and condensate densities with and without the thermal exchange. We look at four temperatures; from top to bottom they are $T/T_{c0} = 0.25$ (dashed), 0.55 (dotted), 0.75 (dash-dotted), and 0.90 (solid). In Fig. 4(a), a Cr gas with (blue) and without (black) the thermal exchange is shown. Additionally, the corresponding condensate density is with (red) and without (green) thermal exchange. This example with the thermal exchange is the same as Fig. 3(a). In Fig. 4(b) a Dy gas with (blue) and without (black) the thermal exchange is shown. The corresponding condensate density is shown with (red) and without (green) thermal exchange. Figure 4(c) shows a comparison of Dy and Cr with a large number of atoms (3700), when the chemical potentials are nearly the same at zero temperature. The densities are normalized to the maximum density at zero temperature.

In Fig. 4(a) the impact of the thermal exchange is not too pronounced. It slightly increases the condensate central density, which is most obvious at high temperature. This is significantly different from the Dy example shown in Fig. 4(b). There is a noticeable difference between the density profiles with and without the thermal exchange. The effect is most clearly seen in the condensate by looking at the increased central density and reduced extent of the red curve (with) versus green (without). At the highest temperature, where the

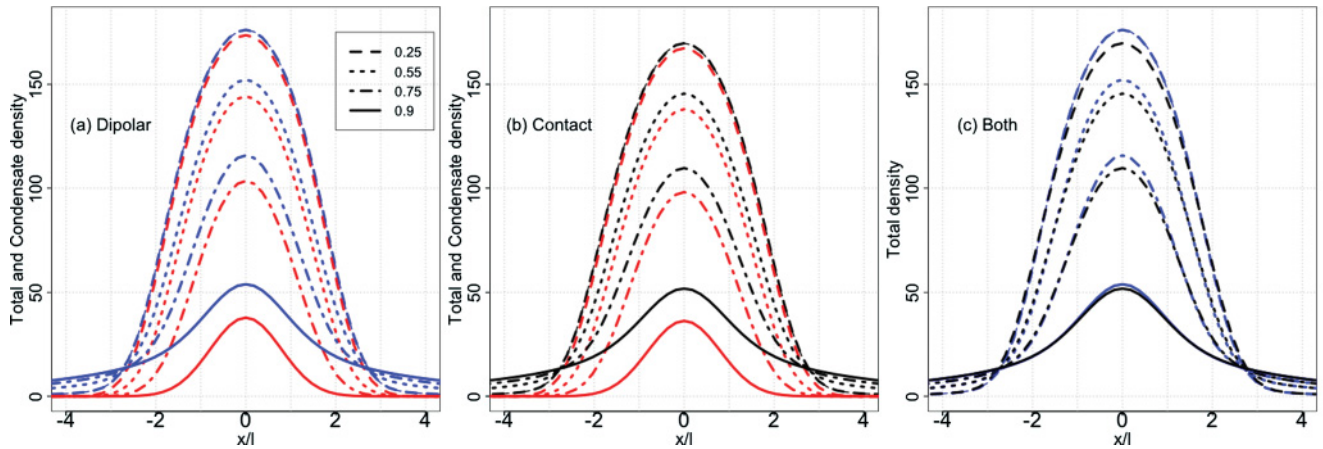

FIG. 3. (Color online) The total and condensate density of (a) a Cr dipolar gas and (b) a contact gas, and the comparison of the total densities (c). The total density is in blue (black) for the dipolar (contact) gas, and the condensate density is in red. The temperatures from top to bottom are $T/T_{c0} = 0.25$ (dashed), 0.55 (dotted), 0.75 (dash-dotted), and 0.90 (solid). (c) The dipolar gas is more dense in the center of the trap at all temperatures.

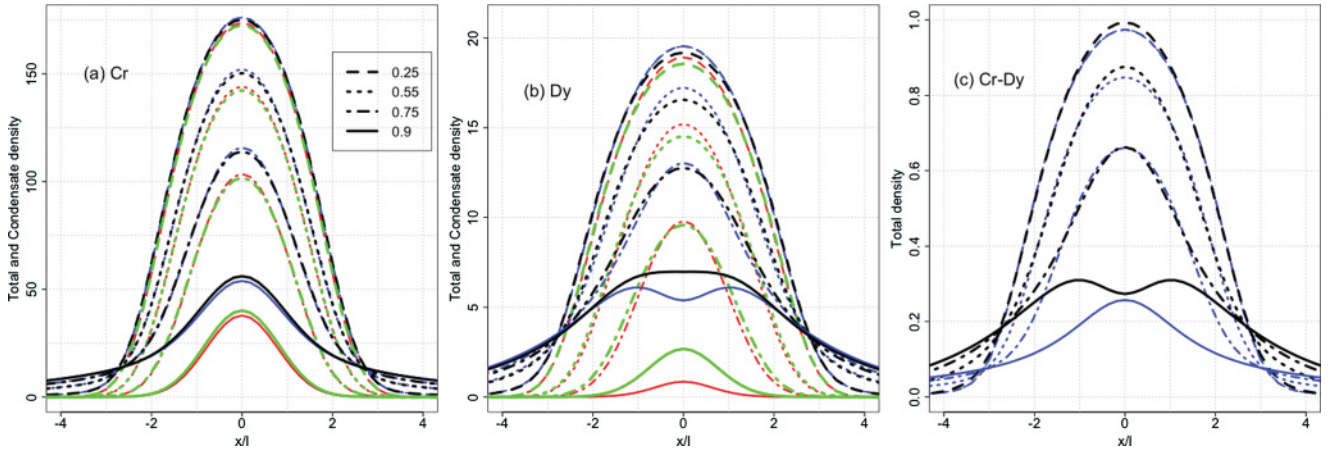

FIG. 4. (Color online) Comparison of densities with and without thermal exchange. Both the total and condensate densities are shown at four temperatures; from top to bottom, $T/T_{c0} = 0.25$ (dashed), 0.55 (dotted), 0.75 (dash-dotted), and 0.90 (solid). (a) A Cr gas with (blue) and without (black) the thermal exchange; the corresponding condensate density with (red) and without (green) thermal exchange is shown. (b) For a Dy gas, the total density with (blue) and without (black) the thermal exchange; the corresponding condensate density with (red) and without (green) thermal exchange is shown. Both the condensate and total densities without thermal exchange have a lower central density. (c) A comparison of Dy (black) and Cr (blue) with a large number of atoms (3700) when the chemical potentials are the same at zero temperature.

validity of the HFBP approximation is questionable, we see a significant reduction in the condensate density and occupation. In fact the condensate repels the thermal cloud so strongly that in the center of the trap there is a local minimum in the total density. Furthermore, the thermal exchange has significantly lowered the condensate occupation. Thus the inclusion of the thermal exchange clearly lowers the critical temperature of the dipolar gas.

In Fig. 4(c) we show that, by varying g_d and N while holding Ng_d constant, the HFBP approximation does not give identical results as the $T = 0$ GPE would. For $g_d = 0.034, N = 300$ (Dy, black) and $g_d = 0.0028, N = 3700$ (Cr, blue) at low temperatures the density profiles are slightly different. More importantly, at high temperature the profiles are very different; this has to do with the strong depletion of the condensate.

In Fig. 5 we show the excitation spectra of the dipolar gas (blue circles), a dipolar gas without the thermal exchange (red triangles), and the contact gas (black pluses) as functions of temperature. We have also characterized the excitations by their azimuthal symmetry. In a 2D contact gas, there is a hidden symmetry which makes the breathing mode ($m = 0$) have an energy of $2\hbar\omega$ [38]. This mode has very little temperature dependence. This hidden symmetry is removed by the dipolar interaction; however, if l_z goes to zero, the breathing mode goes to $2\hbar\omega$. In the example we have picked ($g_d = 0.0028$ and $N = 2000$), the $|m| = 3$ mode is near $2\hbar\omega$, but this is not the breathing mode ($m = 0$). Rather, the mode just below this is the breathing mode. The contact gas excitation spectrum (black pluses) agrees well with that in Ref. [39]. Those authors used $g \sim 0.002$, which accounts for the differences. It is a general feature that the dipolar gas has lower excitation energies than the contact gas. In Ref. [27], the 3D excitation spectrum as a function of temperature showed that for an oblate geometry the dipolar excitations are lower than in the contact system. It is worth pointing out that the dipolar calculations with and without the thermal exchange agree well at low temperature. As the temperature is increased there is some disagreement between the two (blue circles and red triangles), but mostly for more highly excitated modes. The calculations without the exchange become higher in energy.

The modes that have strong temperature dependence are those with higher azimuthal symmetry. In contrast, the full-bodied modes (large central amplitude) have a more constant excitation frequency as the temperature is varied. The reason for this is discussed below.

In Fig. 6 we show the excitation spectrum as a function of N for the dipolar gas (blue circles) at $T/T_{c0} = 0.05$. The plots on the right are contour plots of the quasiparticle modes (u_α)

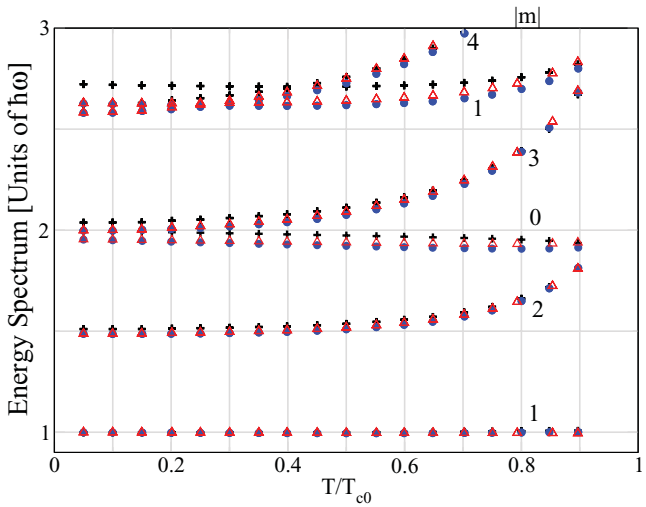

FIG. 5. (Color online) The excitation spectra of the dipolar gas (blue circles), dipolar gas without exchange (red triangles), and contact gas (black pluses) as functions of temperature for $N = 2000$. The azimuthal symmetry of the excitations is shown next to each curve.

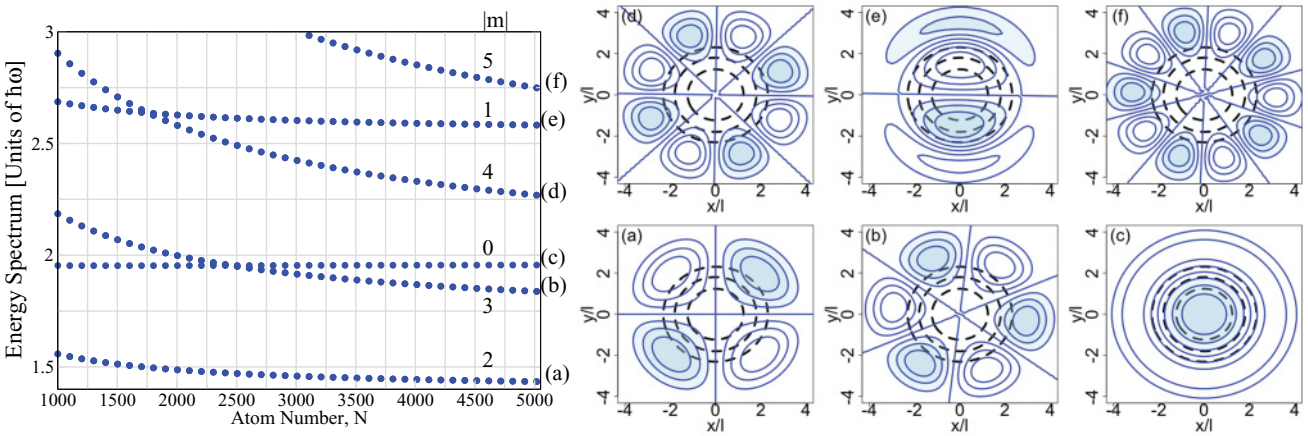

FIG. 6. (Color online) The excitation spectrum as a function of N for the dipolar gas (blue circles) at $T/T_{c0} = 0.05$. The plots on the right are contour plots of the quasiparticle, u_α, modes for $N = 5000$ dipolar atoms. The contour lines are in 0.25 increments of the maximum value of u_α (i.e., 0.75,0.5,. . . , −0.75). Additionally, the negative regions are shaded blue. The condensate density contours (dashed black) are on the same scale.

for $N = 5000$ dipolar atoms. The contour lines are in 0.25 increments of the maximum value of u_α (i.e., 0.75,0.5,. . . , − 0.75). Additionally, the negative regions are shaded blue. The condensate density contours are shown as dashed black lines. The azimuthal symmetries are (a) $m = 2$ quadruple mode, (b) $m = 3$, (c) $m = 0$, breathing mode, (d) $m = 4$, (e) $m = 1$, and (g) $m = 5$. We have shown one of the two degenerate modes ($\pm m$) at each energy when $m \neq 0$. If the contact system were plotted, we would see that the excitations are always higher in energy for all N shown.

The modes that are not strongly dependent on number or temperature are the modes that have a full-bodied motion or large amplitude in the middle of the condensate; see Figs. 6(c) and 6(e). These modes are mildly impacted by the total number of atoms in the system. The modes with higher azimuthal symmetries are more like surface modes and are strongly affected by the number or temperature; see Figs. 6(a), 6(b), 6(d), and 6(f).

In fact the strong number dependence leads to excitations crossing paths as N is increased. The $m = 3$ mode [Fig. 6(b)] becomes lower than the breathing mode [Fig. 6(c)]; and the $m = 4$ mode [Fig. 6(d) becomes lower than the $m = 1$ [Fig. 6(e)]. The fact that surface modes move relative to full-body excitations as a function of N is related to the size of the condensate. Both as the atom number is increased and as the temperature is decreased, the size of the condensate becomes larger. Naively, one might consider the surface of the condensate a ring with a restoring force. We consider the surface excitations as displacements of the ring from equilibrium and find an excitation spectrum which behaves as m/R where R is the radius of the ring [40]. When we look at m over the radius at which the density equals $0.25n_0(0)$ (the furthest out contour of the condensate in Fig. 6), we find a similar number dependence to the excitation spectra in Fig. 6. This is too simplistic, but gives a physical reason for such behavior in the excitation spectrum. The important point of this analysis is that the size of the condensate grows quickly at small N and slows down at larger N. Thus we see a rapid change in the excitation spectrum at low N and less so at large N.

VII. CONCLUSION

This paper studied a trapped Q2D dipolar gases at finite temperature. We presented the numerical method used to solve the Hartree-Fock-Bogoliubov-Popov equations for a gas with nonlocal interactions including thermal exchange effects. It is worth noting that the thermal tail of this gas has the standard form for a 2D gas and could therefore be used for accurate thermometry [2,7]. This is not surprising, but still worth noting for experiments and using as a convergence test for theory.

In Fig. 1 we showed the condensate fraction as a function of temperature for both the Cr and Dy examples. The critical temperature of the Dy is greatly reduced by the interactions. In Fig. 2 we looked at the chemical potential and the total interaction energy as functions of temperature for the various terms in Eq. (1). We compared the contact example with the Cr example with and without thermal exchange. In Fig. 3 we studied the impact of temperature on the density profiles and saw that the dipolar gas is more dense in the center of the trap.

Next, in Fig. 4 we explored the impact of the thermal exchange on both the Cr and Dy examples. We found that, in the strongly interacting Dy example, the thermal exchange strongly reduces the condensate fraction at high temperature. This figure also presented a prediction of this study: when the dipolar interactions are strong and the temperature is near the transition temperature, the total density has a local minimum in the center of the trap where a small condensate strongly expels the thermal atoms. In Fig. 5 we studied the impact of temperature on the excitation spectra. We compared the contact example with the Cr example with and without thermal exchange. Finally, in Fig. 6 we looked at the excitation spectrum of a Cr gas as a function of atom number and the quasiparticles u_α for $N = 5000$. Here we illustrated the strong number or size dependence of the high azimuthal symmetries.

This work has set the stage for studying the phase coherence of a dipolar gas as a function of temperature, as has been done for contact gases [39]. We seek to understand how the nonlocal interaction will alter the correlations at the BKT transition. We

already saw an increased phase-space density in the middle of the cloud from the dipolar interaction. How does the dipolar interaction impact the phase coherence of the gas? Second, we wish to study roton physics in Q2D [28,41,42]. In Q2D, a roton can emerge as the field is tilted into the plane of motion, and leads to anisotropic density profiles [21]. The numerical method presented has been developed to handle this configuration.

This method could be applied to other momentum-dependent interactions, for instance those with renormalized contact interactions, such as $g \rightarrow (g + g^2/k^2)$ [25]. Additionally, we could improve the scattering model to include more dipolar scattering physics [43].

ACKNOWLEDGMENTS

The author gratefully acknowledges support from the Advanced Simulation and Computing Program (ASC) and LANL, which is operated by LANS, LLC for the NNSA of the US DOE under Contract No. DE-AC52-06NA25396. The author acknowledges enlightening discussions with L. A. Collins, R. M. Wilson, A. Sykes, and P. B. Blakie.

[1] V. L. Berezinskii, Sov. Phys. JETP **34**, 610 (1972); L. M. Kosterlitz, D. J. Thouless, J. Phys. C **6**, 1181 (1973).
[2] Z. Hadzibabic and J. Dilibard, Riv. Nuovo Cimento **34**, 389 (2011).
[3] V. Bagnato and D. Kleppner, Phys. Rev. A **44**, 7439 (1991).
[4] Z. Hadzibabic *et al*., Nature (London) **441**, 1118 (2006).
[5] S. Tung, G. Lamporesi, D. Lobser, L. Xia, and E. A. Cornell, Phys. Rev. Lett. **105**, 230408 (2010).
[6] P. Claude, C. Ryu, A. Ramanathan, K. Helmerson, and W. D. Phillips, Phys. Rev. Lett. **102**, 170401 (2009).
[7] C. L. Hung *et al*., Nature (London) **470**, 236 (2011); N. Gemelke, X. Zhang, C.-L. Hung, and C. Chin, *ibid*. **460**, 995 (2009).
[8] N. Prokofev, O. Ruebenacker, and B. Svistunov, Phys. Rev. Lett. **87**, 270402 (2001)
[9] N. Prokof'ev and B. Svistunov, Phys. Rev. A **66**, 043608 (2002).
[10] Z. Hadzibabic *et al*., New J. Phys. **10**, 045006 (2008).
[11] M. Holzmann, M. Chevallier, and W. Krauth, Europhys. Lett. **82**, 30001 (2008).
[12] R. N. Bisset, M. J. Davis, T. P. Simula, and P. B. Blakie, Phys. Rev. A **79**, 033626 (2009).
[13] T. P. Simula, M. J. Davis, and P. B. Blakie, Phys. Rev. A **77**, 023618 (2008).
[14] C. J. Foster, P. B. Blakie, and M. J. Davis, Phys. Rev. A **81**, 023623 (2010).
[15] R. N. Bisset, D. Baillie, and P. B. Blakie, Phys. Rev. A **79**, 013602 (2009); R. N. Bisset, M. J. Davis, T. P. Simula, and P. B. Blakie, *ibid*. **79**, 033626 (2009).
[16] H. P. Buchler, E. Demler, M. Lukin, A. Micheli, N. Prokofev, G. Pupillo, and P. Zoller, Phys. Rev. Lett. **98**, 060404 (2007).
[17] A. Filinov, N. V. Prokofev, and M. Bonitz, Phys. Rev. Lett. **105**, 070401 (2010).
[18] K. Nho and D. P. Landau, Phys. Rev. A **72**, 023615 (2005).
[19] P. Jain, F. Cinti, and M. Bonginsegni, Phys. Rev. B **84**, 014534 (2011).
[20] R. Nath, P. Pedri, and L. Santos, Phys. Rev. Lett. **102**, 050401 (2009).
[21] C. Ticknor, R. M. Wilson, and J. L. Bohn, Phys. Rev. Lett. **106**, 065301 (2011).
[22] M. Lu, N. Q. Burdick, S. H. Youn, and B. L. Lev, Phys. Rev. Lett. **107**, 190401 (2011).
[23] T. Lahaye, J. Metz, B. Fröhlich, T. Koch, M. Meister, A. Griesmaier, T. Pfau, H. Saito, Y. Kawaguchi, and M. Ueda, Phys. Rev. Lett. **101**, 080401 (2008); T. Lahaye, T. Koch, B. Fröhlich, M. Fattori, J. Metz, A. Griesmaier, S. Giovanazzi, and T. Pfau, Nature (London) **448**, 672 (2007); T. Koch, T. Lahaye, J. Metz, B. Fröhlich, A. Griesmaier, and T. Pfau, Nat. Phys. **4**, 218 (2008).
[24] S. Muller, J. Billy, E. A. L. Henn, H. Kadau, A. Griesmaier, M. Jona-Lasinio, L. Santos, and T. Pfau, Phys. Rev. A **84**, 053601 (2011).
[25] A. L. Fetter and J. D. Waleck, *Quantum Theory of Many-Particle Systems* (Dover, New York 2003).
[26] D. S. Jin, J. R. Ensher, M. R. Matthews, C. E. Wieman, and E. A. Cornell, Phys. Rev. Lett. **77**, 420 (1996); M. Edwards *et al*., *ibid*. **77**, 1671 (1996); D. A. W. Hutchinson, E. Zaremba, and A. Griffin, *ibid*. **78** 1842 (1997); R. J. Dodd *et al*., Phys. Rev. A **75**, R32 (1998).
[27] S. Ronen and J. L. Bohn, Phys. Rev. A **76**, 043607 (2007); S. Ronen, D. C. E. Bortolotti, and J. L. Bohn, *ibid*. **74**, 013623 (2006).
[28] S. Ronen, D. C. E. Bortolotti, and J. L. Bohn, Phys. Rev. Lett. **98**, 030406 (2007).
[29] R. N. Bisset, D. Baillie, and P. B. Blakie, Phys. Rev. A **83**, 061602 (2011).
[30] A. Griffin, Phys. Rev. B **53**, 9341 (1996).
[31] B. D. Esry, Phys. Rev. A **55**, 1147 (1997).
[32] Y. Castin and R. Dum, Phys. Rev. A **57**, 3008 (1998); C. Mora and Y. Castin, *ibid*. **67**, 053615 (2003).
[33] S. A. Morgan, Phys. Rev. A **69**, 023609 (2004).
[34] Uwe R. Fischer, Phys. Rev. A **73**, 031602(R) (2006).
[35] P. B. Blakie, C. Ticknor, A. S. Bradley, A. M. Martin, M. J. Davis, and Y. Kawaguchi, Phys. Rev. E **80**, 016703 (2009).
[36] J. Reidl, A. Csordas, R. Graham, and P. Szepfalusy, Phys. Rev. A **59**, 3816 (1999).
[37] T. Bergman, D. L. Feder, N. L. Balazs, and B. I. Schneider, Phys. Rev. A **61**, 063605 (2000).
[38] L. P. Pitaevskii and A. Rosch, Phys. Rev. A **55**, R853 (1997).
[39] C. Gies and D. A. W. Hutchinson, Phys. Rev. A **70**, 043606 (2004); C. Gies, B. P. vanZyl, S. A. Morgan, and D. A. W. Hutchinson, *ibid*. **69**, 023616 (2004).
[40] A. L. Fetter and J. D. Waleck, *Theoretical Mechanics of Particles and Continua* (McGraw-Hill, New York, 1980).
[41] R. M. Wilson, S. Ronen, and J. L. Bohn, Phys. Rev. Lett. **104**, 094501 (2010).
[42] R. M. Wilson, S. Ronen, J. L. Bohn, and H. Pu, Phys. Rev. Lett. **100**, 245302 (2008).
[43] C. Ticknor, Phys. Rev. A **80**, 052702 (2009); **81**, 042708 (2010); **84**, 032702 (2011).